

# Image Deblurring with a Class-Specific Prior

## Supplementary materials

Saeed Anwar, Cong Phuoc Huynh, Fatih Porikli



the blurry edges around the face area. Our proposed algorithm produces acceptable results with far less ringing artifacts.

### 1 CAT IMAGE RECONSTRUCTION

An important aspect we discuss here, is the reconstruction of an example image from Cat dataset [1] using the images from the same dataset. The figure 1 shows the reconstruction results for Cat dataset [1] with some of important filtered training images.

It can be seen that, the algorithm selects a variety of frequency components from different training images to compose the reconstructed image, *i.e.* low-frequency details, mid-frequency details and high-frequency details. Noticeably, the image constructed from the combination of the bandpass components of the training images is free of blur, especially near edges. Most of the mid-frequency to high-frequency components have been recovered. More than five thousand images are used for reconstruction. The reconstructed image lacks smaller details such as whiskers, fur *etc.*

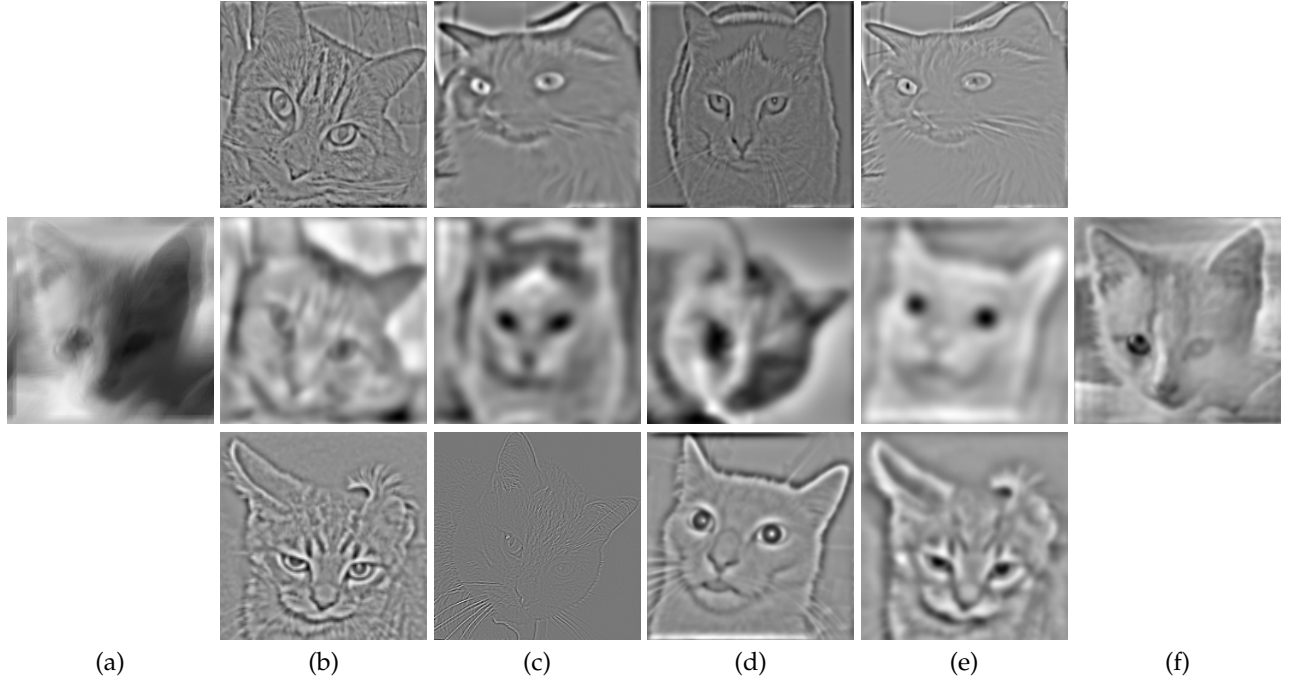


Fig. 1: A visual demonstration of image reconstructed by the weighted combination of all the filtered training images using Cat dataset. (a) Blurred, (b)-(e) important filtered training images, and (f) the reconstructed image.

### 2 MORE DEBLURRING EXAMPLES

In this section, we focus on challenging examples for evaluation of deblurring algorithms. Figure 2 and 3 examples are challenging due to large blur kernels. Figure 2 is a car image with saturation in the rear end. The methods of [2], [3], [4], [5], [6], [7] fails to deblur the image. Our method generates the best result with little to no noise and ringings. Similarly, figure 3 shows the result of our method compared to the state-of-the-art. Here, by incorporating class-specific priors, our method can recover most of the suppressed frequencies compared to competing methods.

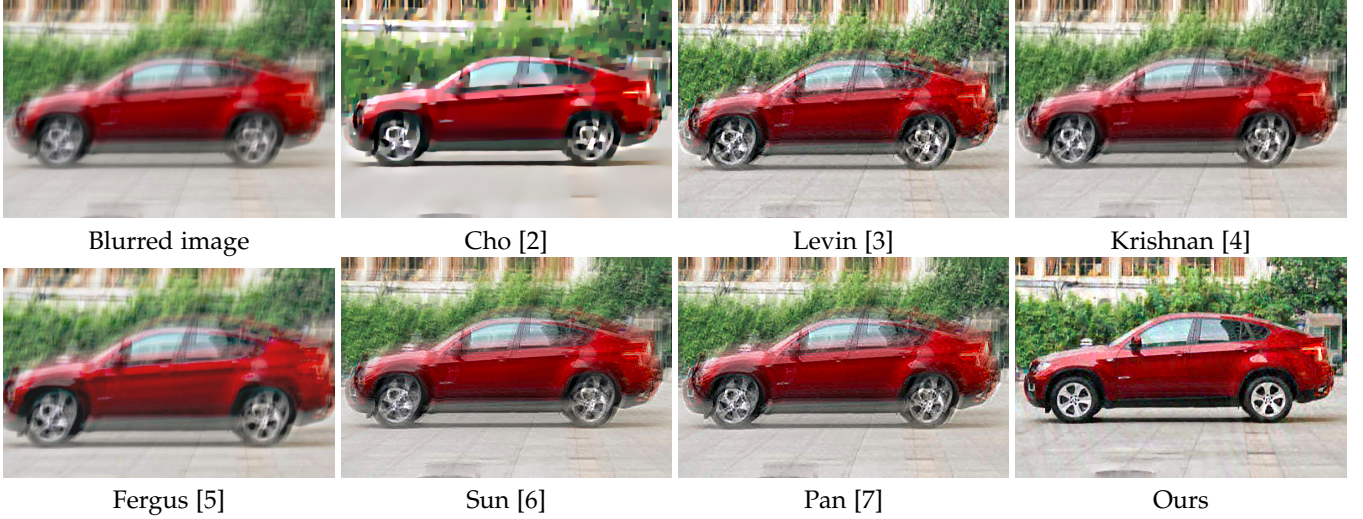


Fig. 2: A challenging blurred example with saturated pixels. Our method has generated the best results without producing any ringing artifacts.

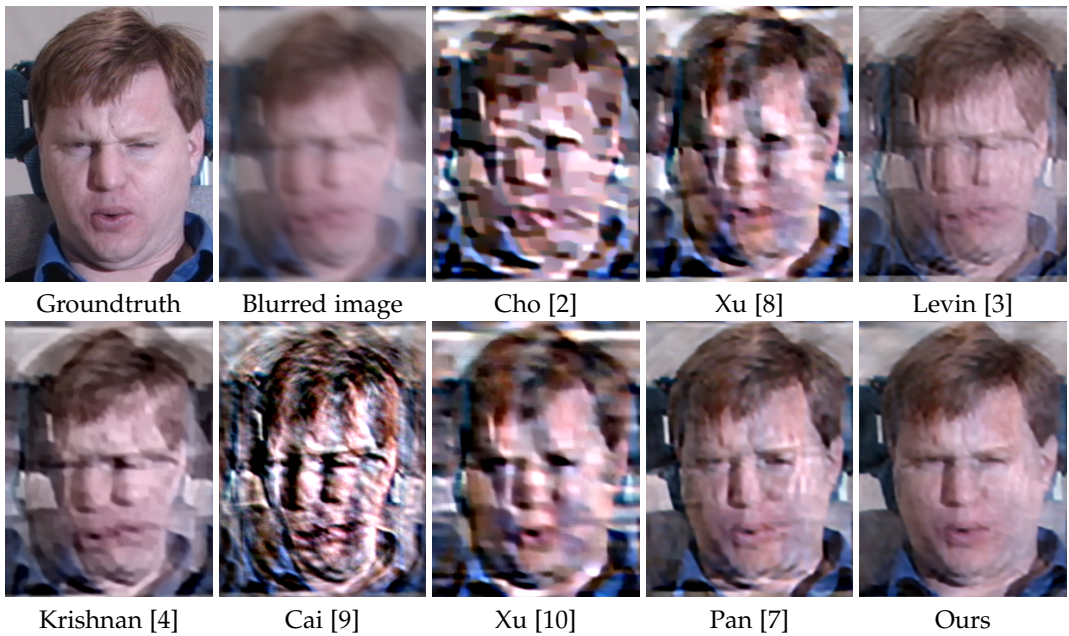


Fig. 3: An extreme blurred image generated synthetically from CMU PIE [11]. Differences can be seen better in high resolution display.

### 3 EXCLUDING LOW FREQUENCIES FROM THE PRIOR

We have performed an experiment where the prior only covers the mid and high frequency bands, and the low frequency components of the latent image are estimated directly from the input image.

Without the low frequency in the prior, the average PSNR for the CMU dataset declines to 25.67 dB, *i.e.* a relative reduction of 16.5% from 30.75 dB (in Table 4 of the main paper, when all the frequency bands are incorporated in the image prior). In addition, Figure 4 demonstrates that the quality of the recovered images degrades when low-frequencies are ignored from the prior.

Hence, incorporating low frequency bands is actually beneficial, rather than harmful, to the deblurring task. As clarified in the previous point, the class-specific low-frequency information has a positive influence on the intermediate kernel estimates, which subsequently improves the image quality produced by the non-blind deconvolution step.

### 4 DISTRIBUTION OF WEIGHTS OF FILTERED TRAINING IMAGES

We plot a 2D colour map (below) for the weights used for the reconstructed image in figure 2. The columns correspond to the contributing images while the rows correspond to the frequency bands. The bands are divided in to low-frequencies



Fig. 4: Different blurry images in first row generated synthetically from [11]. The second row shows the results when only mid and high level frequencies are used, while the results in last row are generated using low, mid and high-frequencies.

(rows 1 to 30), mid-frequencies (row2 31 to 60), and high frequencies (row 61 to 90). The filter weights are colour-coded, where red means high weights and blue means low weights. It can be seen from the plot that high frequency bands contributes the most to the reconstruction, followed by mid and low-frequency bands.

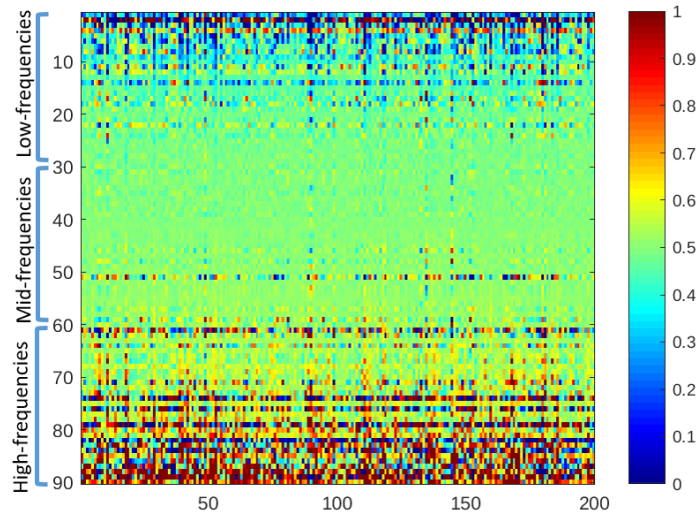


Fig. 5: The weights  $w_{i,j}$  for the reconstruction of the latent image in Figure 2 of the main paper.

## 5 YALE-B IMAGE RECONSTRUCTION ANALYSIS

Another important aspect we discuss in the section is the reconstruction of an example image from Yale-B [12] using the images from the same dataset and Cat dataset [1]. The figure 6 shows the reconstruction results for both Yale-B [12] and Cat dataset [1].

The reconstruction from the training images of Yale-B dataset contains ambiguous features as can be seen near eyebrows and hence results in low PSNR. This maybe due to low-light face images present in the dataset while the reconstruction from the cat images result in smoothing of the features on one side of the face, however, some features are correctly reconstructed, hence, better PSNR.

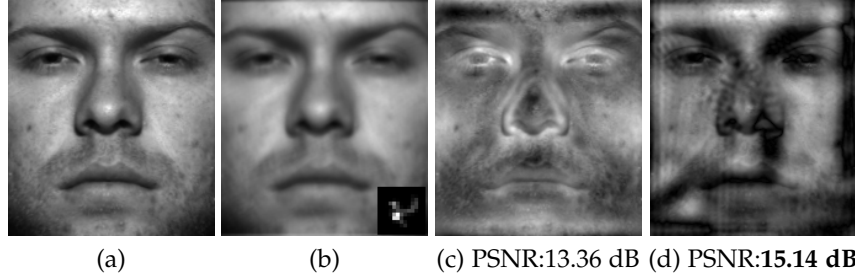


Fig. 6: A visual demonstration of image reconstructed by the weighted combination of all the filtered training images using Yale-B dataset and Cat dataset. (a) Groundtruth, (b) the blurred image with the kernel, (c) the reconstructed image by using Yale-B dataset, and (d) the reconstructed image using Cat dataset. The PSNR is the higher when Cat dataset is used for reconstruction.

## REFERENCES

- [1] W. Zhang, J. Sun, and X. Tang, "Cat head detection-how to effectively exploit shape and texture features," in *ECCV*. Springer, 2008, pp. 802–816.
- [2] S. Cho and S. Lee, "Fast motion deblurring," in *ACM Transactions on Graphics (TOG)*, vol. 28, no. 5, 2009, p. 145.
- [3] A. Levin, Y. Weiss, F. Durand, and W. T. Freeman, "Understanding blind deconvolution algorithms," *TPAMI*, 2011.
- [4] D. Krishnan, T. Tay, and R. Fergus, "Blind deconvolution using a normalized sparsity measure," in *CVPR*, 2011, pp. 233–240.
- [5] R. Fergus, B. Singh, A. Hertzmann, S. T. Roweis, and W. T. Freeman, "Removing camera shake from a single photograph," in *ACM Transactions on Graphics (TOG)*, vol. 25, no. 3, 2006, pp. 787–794.
- [6] L. Sun, S. Cho, J. Wang, and J. Hays, "Edge-based blur kernel estimation using patch priors," in *ICCP*, 2013.
- [7] J. Pan, Z. Hu, Z. Su, and M. Yang, "Deblurring face images with exemplars," in *ECCV*, 2014, pp. 47–62.
- [8] L. Xu and J. Jia, "Two-phase kernel estimation for robust motion deblurring," in *ECCV*, 2010.
- [9] J.-F. Cai, H. Ji, C. Liu, and Z. Shen, "Framelet-based blind motion deblurring from a single image," *Image Processing, IEEE Transactions on*, vol. 21, no. 2, pp. 562–572, 2012.
- [10] L. Xu, S. Zheng, and J. Jia, "Unnatural  $l_0$  sparse representation for natural image deblurring," in *CVPR*, 2013.
- [11] T. Sim, S. Baker, and M. Bsat, "The CMU pose, illumination, and expression (PIE) database," *Automatic Face and Gesture Recognition*, pp. 46–51, 2002.
- [12] A. Georghiades, P. Belhumeur, and D. Kriegman, "From few to many: Illumination cone models for face recognition under variable lighting and pose," *TPAMI*, vol. 23, no. 6, p. 643, 2001.